mathematics

IMPACT FACTOR 2.3

CITESCORE 4.0

Article

Kink Soliton Solutions in the Logarithmic Schrödinger Equation

Tony C. Scott and M. Lawrence Glasser

MDPI

https://doi.org/10.3390/math13050827

mathematics

MDPI

Article

Kink Soliton Solutions in the Logarithmic Schrödinger Equation

Tony C. Scott [1,*,†] and M. Lawrence Glasser [2]

[1] Institut für Physikalische Chemie, RWTH Aachen University, 52056 Aachen, Germany
[2] Department of Physics, Clarkson University, Potsdam, NY 13676, USA
* Correspondence: tcscott@gmail.com
† Current address: Sathorn St-View, 201/1 St Louise 1 Alley, Khwaeng Yan Nawa, Sathon, Bangkok 10120, Thailand.

Abstract: We re-examine the mathematical properties of the kink and antikink soliton solutions to the Logarithmic Schrödinger Equation (LogSE), a nonlinear logarithmic version of the Schrödinger Equation incorporating Everett–Hirschman entropy. We devise successive approximations with increasing accuracy. From the most successful forms, we formulate an analytical solution that provides a very accurate solution to the LogSE. Finally, we consider combinations of such solutions to mathematically model kink and antikink bound states, which can serve as a possible candidate for modeling dilatonic quantum gravity states.

Keywords: logarithmic Schrödinger equation; kink soliton; Everett–Hirschman entropy; nonlinear differential equations; computer algebra

MSC: 81Q05; 34A34; 33B20; 33E05; 68W30; 81P17

1. Introduction

The Logarithmic Schrödinger Equation (LogSE), namely a Schrödinger Equation with logarithmic nonlinearity, has gained significant interest. It has proven to be instrumental for modeling diffusion phenomena [1], quantum optics [2], nuclear physics [3,4], Bose–Einstein Condensates (BECs) [5], superfluids [6–8] fluid mechanics [9,10], classical and quantum gravity [11,12], and Galaxy Rotation curves [13–16]. The LogSE even has geophysical applications in magma transport [17].

In particular, the logarithmic model can account for the *upside-down Mexican hat shape of the Higgs potential*, and its solution is claimed to be even more stable and energetically favorable than the model with a quartic (Higgs-like) potential [18–20] used to understand electroweak symmetry breaking [21].

Bialynicki-Birula et al. established a nonlinear wave mechanics [22] and reported discrete states for the LogSE much in the way of quantum mechanics (QM) as well as soliton solutions known as "Gaussons" [23,24]. Shertzer and Scott found precise numerical solutions for the LogSE in a central Coulomb potential [25,26] and established that a linear combination of Gaussons could be used as an accurate basis for the wave functions. For QM-type solutions, square integrability (L^2 functions) was required of the wave functions satisfying the LogSE.

However, for dilatonic gravity, it is when the dilatonic field is constant, i.e., $\Psi = 1$, that its Lagrangian reduces to the Einstein–Hilbert metric and thus the limit of (classical) General Relativity (GRT) [12]. Thus, local departures from GRT require a dilaton field obeying the LogSE with non-zero far field conditions as constraints. These are not square-integral conditions. For this reason, we consider the "kink" solitons [27] with far field

check for updates

Academic Editor: Emmanuel Yomba

Received: 6 February 2025
Revised: 26 February 2025
Accepted: 27 February 2025
Published: 1 March 2025

Citation: Scott, T.C.; Glasser, M.L. Kink Soliton Solutions in the Logarithmic Schrödinger Equation. *Mathematics* **2025**, *13*, 827. https://doi.org/10.3390/math13050827

conditions that might provide us with a suitable candidate for modeling dilaton fields with local departures from GRT. The purpose of this work is to find precise analytical solutions or rather approximations to the LogSE for "kink" and "antikink" solitons.

We proceed as follows. In Section 2, we identify the differential equation and integral involved and then provide numerical solutions which serve as a benchmark. In Section 3, we examine successive approximations to the main differential approximations, solve them analytically, and compare them. In Section 4, from the most successful of solutions, we infer an analytical form, which turns out to be more precise than all the previous solutions. Finally, we consider combinations of these kink and antikink solutions. A discussion of the results and conclusive comments are made at the end.

2. Logarithmic Scalar Model

The starting point is the $(1+1)$ dimensional Lagrangian density for a real scalar field ([27], Equation (1)).

$$\mathcal{L} = \frac{1}{2}\left(\frac{\partial\phi}{\partial t}\right)^2 - \frac{1}{2}\left(\frac{\partial\phi}{\partial x}\right)^2 - V^0(\phi) \tag{1}$$

where the logarithmic potential $V^0(\phi)$ for a wave function ϕ is given by [27] (Equation (3)):

$$V^0(\phi) = \frac{\phi^2}{\ell^2}\left[\ln(\phi^2/\varphi^2) - 1\right] + \frac{\varphi^2}{\ell^2} \tag{2}$$

The potential in Equation (2) has the proverbial Mexican-hat form, with local minima at $|\phi| = \varphi$ (see the thick black curve in Figure 1a). From the potential in (2), the ordinary differential equation (ODE) for the time-independent case [27] (Equation (5)) is:

$$\frac{d\phi}{dx} = \pm\sqrt{2}\sqrt{V^0(\phi)} = \pm\sqrt{2}\sqrt{\frac{\phi^2}{\ell^2}[\ln(\phi^2/\varphi^2) - 1] + \frac{\varphi^2}{\ell^2}} \tag{3}$$

The $\pm$ is imparted from the fact that $\frac{\partial\phi}{\partial x}$ in (1) is squared. The $+$ (positive) case is found to correspond to the *kink* soliton, while the $-$ (negative) case corresponds to the *antikink* soliton. The differentiation of both sides of (3) with respect to x yields the following:

$$-\frac{1}{2}\frac{d^2\phi}{dx^2} + \frac{1}{\ell^2}\ln\left(\frac{\phi^2}{\varphi^2}\right)\phi = 0 \tag{4}$$

which is a one-dimensional Logarithmic Schrödinger Equation (LogSE) for an eigenvalue of zero. Notice there is no $\pm$ in (4) so both the kink and antikink solitons are solutions to the same LogSE. Also note that the log term in (4) is the *Everett-Hirschman entropy* also called the "Entropic uncertainty" [28–30]. It is defined as the sum of the temporal and spectral Shannon entropies and Heisenberg's uncertainty principle can be expressed as a lower bound on the sum of these entropies.

The constants ℓ and φ can be eliminated by the appropriate choice of units for coordinates and field [27]. Thus, without much loss of generality and for simplicity, we can set $\varphi = 1$ and $\ell = 1$. Separation of variables in the ODE of (3) yields:

$$\pm\frac{1}{\sqrt{2}}\int \frac{1}{\sqrt{\phi^2(\ln(\phi^2) - 1) + 1}}\, d\phi \;=\; x - x_0 \tag{5}$$

where x_0 is a constant. The integral diverges as $1/(\phi - \varphi)$ near its singularity $\phi = \varphi$ (here, $\varphi = 1$). This limits the radius of convergence of series solutions and their usefulness. The integral on the left side is [18] (Equation (30)):

$$\int \frac{1}{\sqrt{\phi^2(\ln(\phi^2)-\epsilon-1)+\exp(\epsilon)}}\,d\phi \tag{6}$$

when the eigenvalue $\epsilon = 0$. No analytical solutions are known for Equation (5), nor for its more general form (6). Equation (5), taken as a definite integral over a defined range $\phi \in [\phi_1, \phi_2]$, which avoids the singularity at $\phi = \varphi = 1$, can be transformed into various forms, such as the following:

$$\begin{aligned}\int_{\phi_1}^{\phi_2} \frac{1}{\sqrt{\phi^2(\ln(\phi^2)-1)+1}}\,d\phi &= \frac{e^{1/2}}{2}\int_{\ln(e/\phi_1^2)}^{\ln(e/\phi_2^2)} \frac{e^{-y/2}}{\sqrt{1-ye^{1-y}}}\,dy \\ &= \frac{e^{1/2}}{2}\int_{\frac{\phi_1^2}{e}\ln(\frac{\phi_1^2}{e})}^{\frac{\phi_2^2}{e}\ln(\frac{\phi_2^2}{e})} \left(\sqrt{\frac{W(k_w,z)}{z(ez+1)}}\right)\frac{dz}{(W(k_w,z)+1)}\end{aligned} \tag{7}$$

where $W(k_w, y)$ is the Lambert W function and k_w is an integer which denotes its choice of branch [31–35]. Since $ye^{1-y} \leq 1$ for $y > 0$, we can apply a binomial expansion to the denominator of the middle form and integrate term by term. This leads to the following series solution.

$$F(x) = -2\sum_{n=0}^{\infty} \frac{e^n(2n)!\Gamma(n+1,(n+1/2)x)}{2^n(n!)^2(2n+1)^{n+1}}\,, \tag{8}$$

where $\Gamma(a, z)$ represents the *incomplete gamma function* [36,37]. Thus, we obtain the following:

$$\int^{y} \frac{e^{-y/2}}{\sqrt{1-ye^{1-y}}}\,dy = F(y) + constant \qquad (y > 1) \tag{9}$$

$$\int_{\phi_1}^{\phi_2} \frac{1}{\sqrt{\phi^2(\ln(\phi^2)-1)+1}}\,d\phi = \frac{e^{1/2}}{2}\Big(\mathrm{sign}(\phi_1)F(\ln(e/\phi_1^2)) - \mathrm{sign}(\phi_2)F(\ln(e/\phi_2^2))\Big)\,.$$

The "switches" $\mathrm{sign}(x_j)$ ensure the $\phi \to -\phi$ symmetry of the integral of (5). The third form of (7) suggests a solution related to a generalized Lambert W function. Note that for the integration range $[\phi_1, \phi_2]$,

$$\phi_2 > \phi_1 > 1 \quad \Rightarrow \quad k_w = 0 \quad W(k_w, y) = W(0, y) \tag{10}$$

$$0 < \phi_1 < \phi_2 < 1 \quad \Rightarrow \quad k_w = -1 \quad W(k_w, y) = W(-1, y)\,. \tag{11}$$

The case $k_w = 0$ represents the Lambert W function on its principal branch, and it is found that the case $k_w = -1$ represents the regime of interest for ϕ. In all cases, exact closed form solutions are not yet possible. Computer algebra systems like Mathematica or Maple [38] cannot produce closed form solutions either, although Maple was used to vindicate the series solution of (8) and (9) both numerically and analytically in the range of interest $0 < \phi_1 < \phi_2 < 1$. However, note that the convergence of the series in (9) slows down and becomes problematic as $\phi_2 \to 1^-$. This may require special summation techniques (as discussed later in Section 3.3). Moreover, we have not obtained a solution of the integral in (5) using the Risch algorithm in Maple. Finally, it should be noted that we seek $\phi(x)$, and (8) is impractical for reversion.

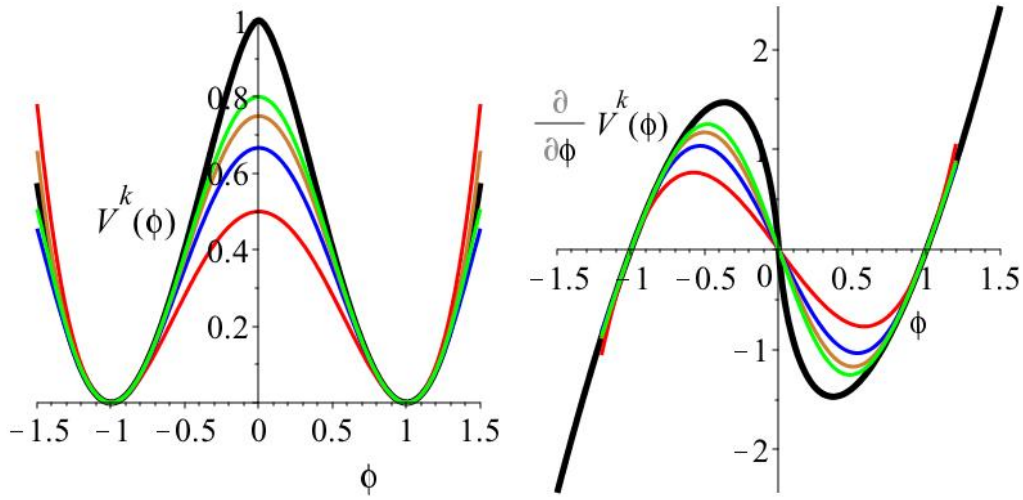

(**a**) (**b**)

Figure 1. (**a**) Potentials $V^k(\phi)$, $k = 0, 1, 2, 3, 4$ in units of φ^2/ℓ^2 versus ϕ in units of φ, where $V^0(\phi)$ is the original logarithmic potential of Equation (2) shown with the black curve, and the $k > 0$ potentials are successive polynomial approximations to $V^0(\phi)$ of Equations (12) and (14). $V^1(\phi)$ of Equation (12) is shown in red. $V^2(\phi)$ is shown in blue. $V^3(\phi)$ is shown in gold. $V^4(\phi)$ is shown in green. (**b**) Corresponding derivatives $\frac{\partial V^k(\phi)}{\partial \phi} k = 0, 1, 2, 3, 4$ vs. ϕ with $\ell = 1$ and $\varphi = 1$ using the same color coding as in (**a**).

Nonetheless, these computer algebra programs give us the means of numerically solving Equation (3). Figure 2 shows both kink and antikink solutions obtained by Maple's numerical ODE solver `dsolve`. The initial conditions for both solutions were set at $\ell = 1$, $\varphi = 1$, $\phi = \pm 0.999941894$ for $x = -5$ to ensure that $\phi(0) = 0$ as much as possible. The solutions of Figure 2 seem to be, at least visually, in agreement with those found in (Ref. [27] Figure 2a). These numerical solutions serve as a benchmark for the approximations of the next section.

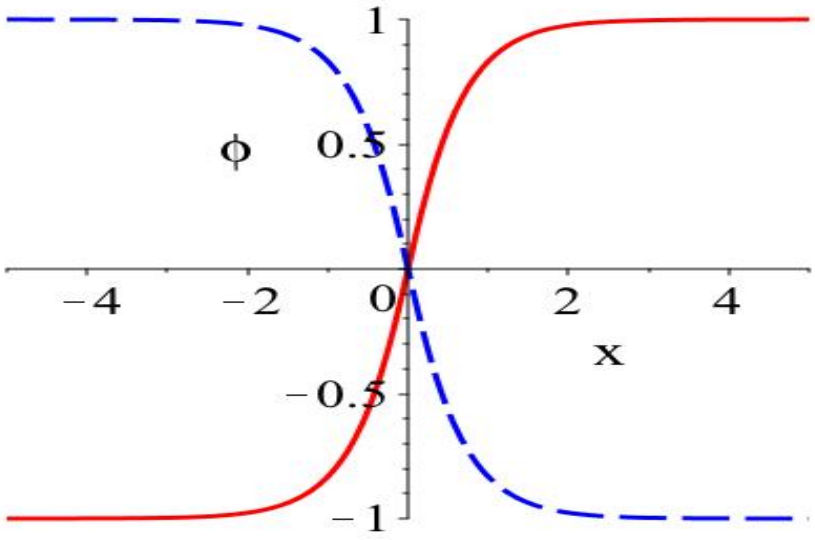

Figure 2. Profiles of the kink (solid red curve) and antikink (dashed blue curve) soliton solutions versus x in units of φ obtained by Maple's numerical ODE solver. $\ell = 1$.

3. Polynomial Approximations of Logarithmic Potential

We consider polynomial approximations of the logarithmic potential, the first being [27] (Equation (4)):

$$V^1(\phi) = \frac{\lambda_H}{4}(\phi^2 - \varphi^2)^2 \quad \text{where} \quad \lambda_H = \frac{2}{\varphi^2 \ell^2} \tag{12}$$

where the subscript "H" refers to the Higgs' quartic ϕ^4 potential. This potential is also shown in Figure 1a in red. Its justification is realized from the Taylor series of the logarithmic potential $V^0(\phi)$ of Equation (2) about $\phi = \varphi$ as follows:

$$\begin{aligned} V^0(\phi) &= \frac{2}{\ell^2}(\phi-\varphi)^2 + \frac{2}{3\varphi\ell^2}(\phi-\varphi)^3 - \frac{1}{6\varphi^2\ell^2}(\phi-\varphi)^4 + \frac{1}{15\varphi^3\ell^2}(\phi-\varphi)^5 \ldots \\ &= \frac{2}{\ell^2}(\phi-\varphi)^2 - \frac{4}{\ell^2}\sum_{i=1}^{\infty}\frac{(-1/\varphi)^i(\phi-\varphi)^{i+2}}{i(i+1)(i+2)}. \end{aligned} \tag{13}$$

A corresponding Taylor series of $V^1(\phi)$ at $\phi = \varphi$ agrees with the Taylor series (13) of V^0 in (13) for the first term, i.e., $k = 1$.

We now consider an extension of ([27] Figure 1) and introduce additional potentials $V^k(\phi)$. These are

$$\begin{aligned} V^2(\phi) &= -\frac{(\phi^2-\varphi^2)^2(\phi^2-4\varphi^2)}{6\ell^2\varphi^4} \\ V^3(\phi) &= \frac{(\phi^2-\varphi^2)^2(\phi^4-4\phi^2\varphi^2+9\varphi^4)}{12\ell^2\varphi^6} \\ V^4(\phi) &= -\frac{(\phi^2-\varphi^2)^2(3\phi^6-14\phi^4\varphi^2+29\phi^2\varphi^4-48\varphi^6)}{60\ell^2\varphi^8} \end{aligned} \tag{14}$$

Like $V^0(\phi)$, all these potentials are symmetric in ϕ, and all are zero at $\phi = \pm\varphi$. These potentials are designed so that a Taylor series of $V^k(\phi)$ about $\phi = \varphi$ agree with the corresponding Taylor series of $V^0(\phi)$ in (13) for the first k terms. Thus, the potentials $V^k(\phi)$ for $k > 0$ are successive polynomial approximations to the original logarithmic potential $V^0(\phi)$.

Figure 1a shows the potentials $V^k(\phi)$, $k = 0, 1, 2, 3, 4$, respectively, in thick black, red, blue, gold, and green. As k grows larger, Figure 1 shows that the potentials $V^k(\phi)$ do indeed increasingly match the initial logarithmic potential $V^0(\phi)$ (shown in thick black) near the peaks at $\phi = 0$, which makes sense. Figure 1b shows the corresponding gradients for these potentials, i.e., $\partial V^k(\phi)/\partial\phi$, $k = 0, 1, 2, 3, 4$ using the same color coding.

The potentials $V^k(\phi)$ have roots beyond $\phi > 1$, causing serious departures of these potentials from $V^0(\phi)$. However, Figure 2 shows us that only the range $\phi \in [-1, 1]$ is of interest and what matters is whether or not, we achieve real analytic functions for $\phi(x)$. Furthermore, the logarithmic potential $V^0(\phi)$ is not Lipschitz continuous [39]. A second derivative for the logarithmic potential $V^0(\phi)$ of (2), with respect to ϕ, diverges to $-\infty$ as $\phi \to 0$, which is in contrast to $V^k(\phi)$ for $k > 0$ since these polynomial approximations are infinitely differentiable. These act as "test functions". This explains how the biggest discrepancies between $V^0(\phi)$ and $V^k(\phi)$ $(k > 0)$ are near $\phi \to 0$. However, we emphasize that the potentials V^k are not, by any means, designed to replace the canonical logarithmic $V^0(\phi)$. Rather, they are a means to an end, which is to find useful successive analytical approximations of the kink and antikink soliton solutions.

3.1. First-Order Approximation V^1 Potential

The ODE to consider is an approximation of (3), namely, the following:

$$\frac{d\phi}{dx} = \pm\sqrt{2}\sqrt{V^1(\phi)} \tag{15}$$

where $V^1(\phi)$ is given in (12). This is readily solved with the Maple system, and the solution is

$$\phi = \pm\tanh(x - x_0) \tag{16}$$

which, qualitatively, looks very much like the numerical solutions of Figure 2. This solution for ϕ is plotted in Figure 3 (in red) and is very close to the accurate numerical solution of (3) (in black). Equation (16) is real and regular for $x \in (-\infty, +\infty)$.

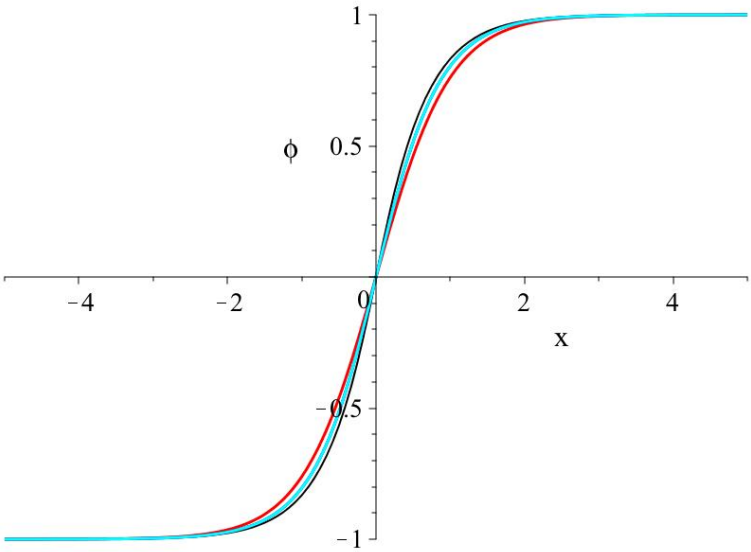

Figure 3. Profiles of the kink solutions versus x for the potentials $V^k(\phi)$, $k = 0, 1, 2$ shown in black, red, blue, respectively, and the ansatz of Equations (22) with (23) is shown in cyan. $\varphi = 1$ and $\ell = 1$.

3.2. Second-Order Approximation V^2 Potential

The ODE to consider is now modified to

$$\frac{d\phi}{dx} = \pm\sqrt{2}\sqrt{V^2(\phi)} \tag{17}$$

where $V^2(\phi)$ is given in (14). Maple's solution uses separation of variables and gives the answer in the form of an integral similar to that of (5) i.e., $x - x_0 = G(\phi)$. It should be appreciated that, quite apart from solving the integral to obtain a solution to an ODE, the latter requires the inversion of $G(\phi)$ to obtain $\phi(x - x_0)$. After a series of manipulations, including the addition law for arctanh functions, we find that the real solutions to (17) are

$$\phi = \pm\frac{\exp(2(x - x_0)) - 1}{\sqrt{\exp(2(x - x_0))^2 + \exp(2(x - x_0)) + 1}} = \pm\frac{\sinh(x - x_0)}{\sqrt{(\cosh(x - x_0))^2 - \frac{1}{4}}} \tag{18}$$

What is interesting about (18) is that, like the previous case for $V_2(\phi)$, we still have a relatively simple solution made of elementary functions, yet a bit more precise than the hyperbolic solution of (16). Equation (18) is also regular since $\cosh(x) \geq 1$ for $x \in (-\infty, +\infty)$. This solution for ϕ is also plotted in Figure 3 in blue and is within the plotting accuracy of the accurate numerical solution of (3).

3.3. Third-Order Approximation V^3 Potential

The ODE to consider is now modified to

$$\frac{d\phi}{dx} = \pm\sqrt{2}\sqrt{V^3(\phi)} \tag{19}$$

where $V^3(\phi)$ is also given in (14). Maple's solution is

$$\pm\frac{\sqrt{3}}{3}\left(\sqrt{5}-i\right)EllipticPi\left(\frac{(\sqrt{2}\,i+\sqrt{10})}{6}\phi, 2-i\sqrt{5}, \frac{2-i\sqrt{5}}{3}\right) = x - x_0 \tag{20}$$

where $i^2 = -1$ and Maple's `EllipticPi` (or Π) is the (3-argument) incomplete elliptic integral. Though expressed in the complex plane, Equation (20) is real for $\phi \in (-1, 1)$. Unfortunately, the elliptic function is not easy to invert, especially with complex arguments, and we have, so far, no means of simplifying (20) to simpler functions. Nonetheless, we verified that the solution of Equation (20) is closer to in accuracy to the solution of (3) than Equations (16) or (18).

Maple gives us the means to achieve a series expansion of $EllipticPi(z, \nu, \mu)$ in its first argument z, allowing the left side of (20) to be expanded as a real series in powers of ϕ. Maple also gives us the means to reverse to the latter to obtain ϕ as a power series in x. Unfortunately, the resulting series in x is divergent and requires high-power summation techniques such as the Levin and Sidi transformation. The Maple package `trans` [40] was instrumental in this case and allowed us to obtain a rational function in x for ϕ within plotting accuracy for the range $x \in (-2, 2)$. This was enough to give us confidence in the solution. However, unless or until (20) can be considerably simplified, it is not yet practical.

3.4. Fourth-Order Approximation V^4 Potential

The ODE to consider is now modified to

$$\frac{d\phi}{dx} = \pm\sqrt{2}\sqrt{V^4(\phi)} \tag{21}$$

where $V^4(\phi)$ is the final function in the list of (14). Maple's solution is similar to that of Equation (20). It is also in the complex plane. However, it is far bigger. It not only involves Maple's `EllipticPi` as before but also includes "EllipticF", which is the incomplete elliptic integral of the first kind. Due to limitations in length, we do not present the solution here. As in (20), it is also of the form $x - x_0 = G(\phi)$ and is even more difficult to invert to obtain $\phi(x)$. As such, it is not useful, and there is no point in further iterations. The approximations reached their maximum in usefulness with $V^2(\phi)$, namely Equation (18).

4. Results

Figure 3 compares the numerical kink solution of Figure 2 with the successive analytical solutions of Equation (16) (shown in red) and (18) (shown in blue). As we can see, they are rather good.

4.1. Empirical Model

Given that V^2 with its solution for ϕ in (16) and V^3 with its solution for ϕ in (18) provide the simplest and most effective solutions, we consider the following general model:

$$\phi = \pm\frac{\sinh(x - x_0)}{\sqrt{(\cosh(x - x_0))^2 - A^2)}} \quad \text{where} \quad |A| < 1\,. \tag{22}$$

Here, we introduced the parameter A. When $A = 0$, Equation (22) reduces to the hyperbolic solution of (16), and when $A = 1/2$, it becomes (18). Thus, it is a matter of refining A by obtaining (22) for $x \in (-5, 5)$ and comparing the results to the accurate numerical solution(s) shown in (2). The constraint on A ensures that the denominator of (22) never becomes zero, so this solution remains real and continuous over $x \in (-\infty, +\infty)$. From the resulting plot of $A = A(x - x_0)$, we find that it best suits the following form:

$$A = A(x - x_0) = a_0 + b_0 \exp(-c|x - x_0|) \quad \text{where} \quad c > 0 \quad \text{and} \quad |a_0 + b_0| < 1\,. \tag{23}$$

The coefficients a_0, b_0, and c are obtained by a least squares fit. We empirically found that $a_0 = 0.5955$, $b_0 = 0.12462$, and $c = 1.52225$ yield the smallest RMS error in comparison to all the solutions obtained from V^k for $k = 1, 2, 3, 4$. The resulting solution (22) with (23) is shown in cyan in Figure 3. This solution satisfies both sides of the ODE in (3) to about three digits over the region $x \in (-5, 5)$, which is better than plotting accuracy for the full range shown in Figure 3. Note that A in (23) reaches its maximal value at $x = x_0$, i.e., at $A = a_0 + b_0 = 0.5955 + 0.12462 = 0.7212$, which is below unity. Thus, the denominator of (22) can never reach zero for $x \in (-\infty, +\infty)$.

In view of (23), it becomes very difficult to invert (22) to obtain x in terms of ϕ which is used to express an approximate solution of (5). This inversion leads to solving an expression made of powers in $\exp(\phi)$, and when c is not an integer, some of these powers are not whole numbers. At any rate, a solution to this expression suggests a yet unknown generalization of the Lambert W function [41]. Though this is perhaps not conclusive from the point of view of Pure Mathematics, our efforts, nonetheless, suggest that, if there is a solution for (5), it is likely in terms of a special function, perhaps a generalized Lambert W function, with an inverse that is only approximated by (22).

4.2. Products of Wave Functions

As mentioned before, linear combinations of Gaussons can well approximate the solutions of the LogSE for central potentials [25,26]. Moreover, Carles and Ferrière established a quasi nonlinear property of superposition which has been firmly established for quadratic potentials [39]. Ref. [27] (Equation (14)) considers linear combinations of kink and antikink solutions for their own bion model based on the LogSE. Instead, we consider *products* of such functions, given the well-known property of logarithms:

$$\ln(\Psi(x)\Phi(x)) = \ln(\Psi(x)) + \ln(\Phi(x)) \tag{24}$$

If Ψ and Φ peak in different locations, the logarithm acts as a separator much like "Cepstral" analysis used in Audio Engineering to separate functions in different frequency regimes [42,43]. In such a case, the Laplacian of this product actually separates since in the far-field, kink and antikink reach constants ± 1, as shown in the following:

$$\frac{\partial^2(\Psi(x)\Phi(x))}{\partial x^2} = \frac{\partial^2\Psi(x)}{\partial x^2}\Phi(x) + 2\underbrace{\left(\frac{\partial\Psi(x)}{\partial x}\right)\left(\frac{\partial\Phi(x)}{\partial x}\right)}_{\approx 0} + \Psi(x)\frac{\partial^2\Phi(x)}{\partial x^2} \tag{25}$$

Thus, the product of the gradients of $\Psi(x)$ and $\Phi(x)$ are nearly zero if their respective centers are sufficiently far apart. This property, along with (24), allow for a separation of the LogSE on the product $\Psi(x)\Phi(x)$ into individual LogSEs for each of these functions. To demonstrate the consequences, Figure 4a shows the product of such functions separated by a distance of 10 units, while Figure 4b shows the product of the gradients, i.e., first derivatives of $\Psi(x)$ and $\Phi(x)$ with respect to x. This is shown for the various analytical soliton solutions shown so far, i.e., Equations (16) (in red), (18) (in blue), and (22) with (23)

(in cyan). For Figure 4a, the products of the wave functions $\phi(x-5) * \phi(x+5)$ are within plotting accuracy. For Figure 4b, the products of the gradients, $\phi'(x-5) * \phi'(x+5)$ where the prime $(')$ denotes derivative with respect to x are all very small, within the magnitude of about 10^{-8} units. It becomes smaller as the analytical soliton solutions become more accurate. This assures assuring that products of kink and/or antikink solitons are rather good approximate solutions of the LogSE, and many scenarios of such soliton combinations can be envisaged. Figure 4a is an example of shows a local departure from a constant field that obeys the LogSE and resembles one of the solutions ([27] Figure 5).

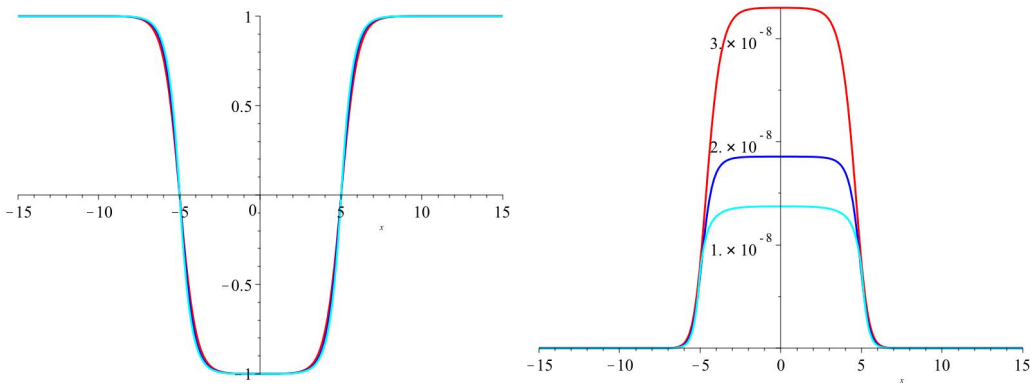

(**a**) (**b**)

Figure 4. (**a**) Product of wave functions centered at $x = \pm 5$ i.e., $\phi(x-5) * \phi(x+5)$. (**b**) Product of derivatives of these same wave functions. $\phi = tanh$ shown in red, ϕ given by (18) shown in blue, and ϕ given by (22) and (23) shown in cyan.

5. Discussion and Conclusions

Our analysis has yielded some practical and useful approximate analytical solutions of the LogSE for kink and antikink soliton solutions. In this regard, the solutions of Equation (16) and especially the slightly more accurate Equation (18) are dividends of this study—sufficiently accurate yet relatively simple soliton solutions in terms of elementary functions.

To reiterate, the solutions from the potentials $V^1(\phi)$ and $V^2(\phi)$ achieved useful practical results, although $V^3(\phi)$ and $V^4(\phi)$ yielded diminishing returns. However, from the solutions of $V^1(\phi)$ and $V^2(\phi)$, we inferred a functional form in terms of elementary functions that turned out to be very accurate yet rather simple.

Another dividend, as shown in Section 4.2, is how one can take products of individual soliton solutions to create more sophisticated departures from constant fields. Figure 4a is only one example of the various combinations one can make for kink or antikink solutions while retaining continuity and satisfying the LogSE.

Of course, so far, we have only considered static one-dimensional problems. However, the logarithmic property of (24) also allows us to separate time-varying 3D problems in, e.g., their respective Cartesian coordinates. So far, we have not really discussed the Physics involved in creating kink-antikink combinations. Like many soliton solutions, their creation is often an issue of imparting the right boundary conditions. Ref. [27] provides a number of time-dependent simulations, e.g., scattering cases while considering the ebb and flow of kinetic energy. It is interesting how the Everett–Hirschman entropy (not being Lipschitz continuous when its argument is zero) imparts élan into the Schrödinger equation to produce these kink and antikink solitons. The lack of Lipschitz continuity, i.e., indeterminism at $\phi = 0$ in the logarithmic term of the LogSE, may very well explain the spontaneous symmetry breaking phenomenon [18]. However, our focus has been on mathematical solutions. In conclusion, our mathematical study provides us with simple

and effective functional forms to model kink and antikink soliton solutions and their combination, for a wide range of cases.

Author Contributions: Software, T.C.S.; Formal analysis, T.C.S. and M.L.G.; Investigation, T.C.S. All authors have read and agreed to the published version of the manuscript.

Funding: This research received no external funding.

Data Availability Statement: Data are contained within the article.

Acknowledgments: We would like to express our thanks to K. G. Zloshchastiev for his feedback.

Conflicts of Interest: The authors declare no conflicts of interest.

Abbreviations

The following abbreviations are used in this manuscript:

BEC	Bose–Einstein Condensates
GRT	General Relativity
LogSE	Logarithmic Schrödinger Equation
ODE	Ordinary Differential Equations
QM	Quantum Mechanics

References

1. Hansson, T.; Anderson, D.; Lisak, M. Propagation of partially coherent solitons in saturable logarithmic media: A comparative analysis. *Phys. Rev. A* **2009**, *80*, 033819. [CrossRef]
2. Buljan, H.; Šiber, A.; Soljačić, M.; Schwartz, T.; Segev, M.; Christodoulides, D.N. Incoherent white light solitons in logarithmically saturable noninstantaneous nonlinear media. *Phys. Rev. E* **2003**, *68*, 036607. [CrossRef] [PubMed]
3. Hefter, E.F. Application of the nonlinear Schrödinger equation with a logarithmic inhomogeneous term to nuclear physics. *Phys. Rev. A* **1985**, *32*, 1201–1204. [CrossRef]
4. Kartavenko, V.G.; Gridnev, K.A.; Greiner, W. Nonlinear Effects in Nuclear Cluster Problem. *Int. J. Mod. Phys. E* **1998**, *07*, 287–299. [CrossRef]
5. Avdeenkov, A.V.; Zloshchastiev, K.G. Quantum Bose liquids with logarithmic nonlinearity: Self-sustainability and emergence of spatial extent. *J. Phys. At. Mol. Opt. Phys.* **2011**, *44*, 195303. [CrossRef]
6. Scott, T.C.; Zloshchastiev, K.G. Resolving the puzzle of sound propagation in liquid helium at low temperatures. *Low Temp. Phys.* **2019**, *45*, 1231–1236. [CrossRef]
7. Zloshchastiev, K.G. Volume element structure and roton-maxon-phonon excitations in superfluid helium beyond the Gross-Pitaevskii approximation. *Eur. Phys. J. B* **2012**, *85*, 273. [CrossRef]
8. Zloshchastiev, K.G. Resolving the puzzle of sound propagation in a dilute Bose-Einstein condensate. *Int. J. Mod. Phys. B* **2022**, *36*, 2250121. [CrossRef]
9. Zloshchastiev, K.G. Nonlinear wave-mechanical effects in Korteweg fluid magma transport. *Europhys. Lett.* **2018**, *122*, 39001. [CrossRef]
10. Ván, P. Holographic fluids: A thermodynamic road to quantum physics. *Phys. Fluids* **2023**, *35*, 057105. [CrossRef]
11. Zloshchastiev, K.G. Logarithmic nonlinearity in theories of quantum gravity: Origin of time and observational consequences. *Gravit. Cosmol.* **2010**, *16*, 288–297. [CrossRef]
12. Scott, T.C.; Zhang, X.; Mann, R.B.; Fee, G.J. Canonical reduction for dilatonic gravity in 3+1 dimensions. *Phys. Rev. D* **2016**, *93*, 084017. [CrossRef]
13. Zloshchastiev, K.G. An Alternative to Dark Matter and Dark Energy: Scale-Dependent Gravity in Superfluid Vacuum Theory. *Universe* **2020**, *6*, 180. [CrossRef]
14. Zloshchastiev, K.G. On Asymptotic Behavior of Galactic Rotation Curves in Superfluid Vacuum Theory. *Astron. Rep.* **2021**, *65*, 1078–1083. [CrossRef]
15. Zloshchastiev, K.G. Galaxy rotation curves in superfluid vacuum theory. *Pramana-J. Phys.* **2022**, *97*, 2. [CrossRef]
16. Scott, T.C. From Modified Newtonian Dynamics to Superfluid Vacuum Theory. *Entropy* **2023**, *25*, 12. [CrossRef]
17. Lauro, G. A note on a Korteweg fluid and the hydrodynamic form of the logarithmic Schrödinger equation. *Geophys. Astrophys. Fluid Dyn.* **2008**, *102*, 373–380. [CrossRef]

18. Zloshchastiev, K.G. Spontaneous Symmetry Breaking and Mass Generation as Built-in Phenomena in Logarithmic Nonlinear Quantum Theory. *Acta Phys. Pol. B* **2011**, *42*, 261. [CrossRef]
19. Dzhunushaliev, V.; Zloshchastiev, K. Singularity-free model of electric charge in physical vacuum: Non-zero spatial extent and mass generation. *Open Phys.* **2013**, *11*, 325–335. [CrossRef]
20. Dzhunushaliev, V.; Makhmudov, A.; Zloshchastiev, K.G. Singularity-free model of electrically charged fermionic particles and gauged *Q*-balls. *Phys. Rev. D* **2016**, *94*, 096012. [CrossRef]
21. Itzykson, C.; Zuber, J.B. *Quantum Field Theory*; Dover Books on Physics, Dover Publications: Mineola, NY, USA, 2006.
22. Bialynicki-Birula, I.; Mycielski, J. Nonlinear wave mechanics. *Ann. Phys.* **1976**, *100*, 62–93. [CrossRef]
23. Bialynicki-Birula, I.; Mycielski, J. Gaussons: Solitons of the Logarithmic Schrödinger Equation. *Phys. Scr.* **1979**, *20*, 539. [CrossRef]
24. Bialynicki-Birula, I.; Sowiński, T., Solutions of the Logarithmic Schrödinger Equation in a Rotating Harmonic Trap. In *Nonlinear Waves: Classical and Quantum Aspects*; Springer: Dordrecht, The Netherlands, 2005; pp. 99–106. [CrossRef]
25. Scott, T.C.; Shertzer, J. Solution of the logarithmic Schrödinger equation with a Coulomb potential. *J. Phys. Commun.* **2018**, *2*, 075014. [CrossRef]
26. Shertzer, J.; Scott, T.C. Solution of the 3D logarithmic Schrödinger equation with a central potential. *J. Phys. Commun.* **2020**, *4*, 065004. [CrossRef]
27. Belendryasova, E.; Gani, V.A.; Zloshchastiev, K.G. Kink solutions in logarithmic scalar field theory: Excitation spectra, scattering, and decay of bions. *Phys. Lett. B* **2021**, *823*, 136776. [CrossRef]
28. Białynicki-Birula, I.; Mycielski, J. Uncertainty relations for information entropy in wave mechanics. *Commun. Math. Phys.* **1975**, *44*, 129–132. [CrossRef]
29. Zloshchastiev, K.G. On the Dynamical Nature of Nonlinear Coupling of Logarithmic Quantum Wave Equation, Everett-Hirschman Entropy and Temperature. *Z. Fuer Naturforschung A* **2018**, *73*, 619–628. [CrossRef]
30. Zloshchastiev, K.G. Origins of Logarithmic Nonlinearity in the Theory of Fluids and Beyond. [CrossRef]
31. Corless, R.M.; Gonnet, G.H.; Hare, D.E.G.; Jeffrey, D.J.; Knuth, D.E. On the LambertW function. *Adv. Comput. Math.* **1996**, *5*, 329–359. [CrossRef]
32. Scott, T.C.; Mann, R.; Martinez, R.E., II. General Relativity and Quantum Mechanics: Towards a generalization of the Lambert W function. *Appl. Algebra Eng. Commun. Comput.* **2006**, *17*, 41–47. [CrossRef]
33. Scott, T.C.; Fee, G.; Grotendorst, J. Asymptotic series of generalized Lambert W function. *ACM Commun. Comput. Algebra* **2014**, *47*, 75–83. [CrossRef]
34. Scott, T.C.; Fee, G.; Grotendorst, J.; Zhang, W.Z. Numerics of the generalized Lambert W function. *ACM Commun. Comput. Algebra* **2014**, *48*, 42–56. [CrossRef]
35. Maignan, A.; Scott, T.C. Fleshing out the Generalized Lambert W Function. *ACM Commun. Comput. Algebra* **2016**, *50*, 45–60. [CrossRef]
36. Abramowitz, M. *Handbook of Mathematical Functions, With Formulas, Graphs, and Mathematical Tables*; Dover Publications, Inc.: Mineola, NY, USA, 1974.
37. Geddes, K.O.; Glasser, M.L.; Moore, R.A.; Scott, T.C. Evaluation of classes of definite integrals involving elementary functions via differentiation of special functions. *Appl. Algebra Eng. Commun. Comput.* **1990**, *1*, 149–165. [CrossRef]
38. Bernardin, L.; Chin, P.; Demarco, P.; Geddes, K.O.; Hare, D.E.G.; Heal, K.M.; Labahn, G.; Mccarron, J.; Monagan, M.B.; Ohashi, D.; et al. *Maple Programming Guide*; Maplesoft: Waterloo, ON, Canada, 2011.
39. Carles, R.; Ferrière, G. Logarithmic Schrödinger equation with quadratic potential. *Nonlinearity* **2021**, *34*, 8283. [CrossRef]
40. Grotendorst, J. TRANS: A Maple Package for Transforming Series, Sequences and Functions. In Proceedings of the 13th IMACS World Congress on Computation and Applied Mathematics. 13th IMACS World Congress on Computation and Applied Mathematics, Dublin, Ireland, 22–26 July 1990; pp. 95–97.
41. Scott, T.C.; Aubert-Frécon, M.; Grotendorst, J. New approach for the electronic energies of the hydrogen molecular ion. *Chem. Phys.* **2006**, *324*, 323–338. [CrossRef]
42. Bogert, B.P.; Healy, J.R.; Tukey, J. The Quefrency Analysis of Time Series for Echoes: Cepstrum, Pseudo-Autocovariance, Cross-Cepstrum, and Saphe Cracking. In *Proceedings of the Symposium on Time Series Analysis*; Wiley: Hoboken, NJ, USA, 1963; pp. 209–243.
43. Bauman, P.D.; Lipshitz, S.P.; Scott, T.C.; Vanderkooy, J. Cepstral techniques for transducer measurement. In Proceedings of the Presented at the 76th Convention AES, New York, NY, USA, 8–11 October 1984; Volume 2172, pp. 1–43.